Determination of principal characteristics of turbulent swirling flow along annuli

Part 3: Numerical analysis

Y. S. M. Morsi* and B. R. Clayton**

Turbulent swirling flow along the axisymmetric annulus formed between two co-axial tubes of different diameter but the same length is considered. All boundary layers are considered to be removed at entry to the test section for consistency with the authors' experimental data. A description is given of the flow development along the test section to a region where fully developed flow may be assumed, and both large and small swirl components are examined. The analysis commences from a general statement of the Navier–Stokes equations in cylindrical coordinates written in a form to account for turbulent velocity components. A technique for the solution of the resulting elliptic equations and associated boundary conditions is presented, and the results compared with experimental and other analytic data. It is necessary to adopt a model to describe the spatial dependence of the turbulence parameters, and investigations using both the concept of a mixing length and a k–ε model are described. Good agreement between theory and experiment in respect of velocity profiles is obtained, and the successive improvement in predictions with increased sophistication of turbulence models is demonstrated.

Keywords: *turbulence, swirling flow, elliptic Navier–Stokes equations, finite difference techniques, numerical analysis, co-axial tubes*

Introduction

In previous papers[1,2] the authors have presented experimental data for both time-mean and turbulence parameters, describing the development along an axisymmetric annulus of an initially inviscid swirl flow at entry. This type of flow has important applications in, for example, the design of heat exchangers, combustion chambers and turbomachinery. In this paper a description is given of swirling flows between two concentric, stationary tubes with a common entry plane. Some work has been performed on a similar geometry, but with rotation of the inner tube about the common generator axis[3].

Although this paper is primarily concerned with turbulent swirling flow in an annulus, some special cases are also examined in order to test the general analytical procedures. In particular, laminar flow and pipe geometry are included. A full discussion of the techniques adopted by various authors dealing with relevant flow problems has been given by Morsi[4], and so here we select a few of special interest. Scott[5], for example, has dealt with the characteristics of the decay of swirling turbulent flow in pipes and annuli. He assumed the flow to be fully developed, ie the axial flow velocity profile was of constant shape, and was then able to reduce the simplified partial differential equation into one of ordinary derivatives. Kreith and Sonju[6] have dealt with fully developed turbulent pipe swirl flow.

Many formidable fluid dynamics problems have been tackled successfully in recent years using high speed computers to accommodate a variety of numerical techniques. Patankar and Spalding[7] have developed a method of solving the differential equations for turbulent boundary layer flows using a finite difference procedure. A computer program, referred to as GENMIX, has now been made available[7]. There have been various applications of the analytical approach which essentially requires the solution of the parabolic form of the momentum equations (which can only be applied to a flow with no region of reverse or secondary flows). The method was used by Sharma *et al*[3] and reasonable agreement with experiments was reported. More recently, Yamamoto and Millar[8] have used the parabolized Navier–Stokes equations with the Crank–Nicholson finite difference scheme and a k–ε turbulence model to predict turbulent swirling flow entering a stationary annulus. They compared their predictions with the experimental data of Scott and Rask[9]. However, in this case, poor agreement with measurements was found and further study was recommended.

There is little doubt that turbulent swirling flows can best be described by the elliptic form of Navier–Stokes equations (particularly flow of high swirl and recirculation). A finite difference procedure to solve the steady form of these elliptic equations has been published

* Department of Mechanical Engineering, Loughborough University of Technology, Loughborough
** Department of Mechanical Engineering, University College, London

0142–727X/86/030208–15$3.00

by Gosman *et al*[10]. For this technique an up-wind difference scheme is used to approximate the convection terms. It is then possible to ensure that the matrices containing the coefficients of sets of finite difference equations are unconditionally diagonally dominant, thus promoting numerical stability and speedy convergence of the solution, particularly for flow at high Reynolds numbers. Several investigators have used this approach for various swirl flow problems, eg Kubo and Gouldin[11]. for a combustion swirl chamber, Crane and Burley[12] for laminar swirl in a diffuser, and Huang and Tsou[13] for turbulent free-swirling pipe flows and heat transfer.

In what follows, we apply the numerical technique of Gosman *et al*[10] to turbulent swirling flow in a constant section annulus and introduce the necessary modifications to satisfy the boundary conditions imposed by the geometry of the confining tubes. A measure of the success of the theoretical predictions is obtained from a comparison with experimental data[1] and other analytical data where available. A discussion of the effect of turbulence models (MLH and k–ε) on the predicted data is also given.

Equations of motion

The fluid is considered to be incompressible and the flow isothermal and axially symmetric, ie the axis no circumferential variation of flow properties at a given radius in a given plane perpendicular to the axis of symmetry of the annular test section. Furthermore, the flow possesses steady mean components upon which are *impressed* turbulence fluctuations. The cylindrical coordinate system used is shown in Fig 1, where $\tilde{U}$, $\tilde{V}$ and $\tilde{W}$ are the axial, radial and tangential velocities corresponding to the axial, radial and tangential coordinates x, r, θ. Here we assume $\tilde{U}$ to be made up of a time average component $\bar{U}$ and a turbulence fluctuation component u', and similarly for the other velocities, ie

$$\tilde{U}=\bar{U}+u' \qquad \tilde{V}=\bar{V}+v' \qquad \tilde{W}=\bar{W}+w' \tag{1}$$

Notation

A	Cross-sectional area of annulus $\equiv\pi(r_o^2/r_i^2)$
A'	Empirical constant
A_Φ, B_Φ, C_Φ, D_Φ	Functions in Eq (31), defined in Table 3
a_ϕ, b_ϕ, c_ϕ, d_ϕ	Functions in Eq (28), defined in Table 2
C_1, C_2, C_D, C_x, C_μ	Emprical constants
F_μ	Function defined by Eq (25)
F'_μ	r_oF_μ/U_{av}
G	Generation term for kinetic energy defined by Eq (19)
K, K_C	Empirical constants
k	Turbulence kinetic energy per unit mass
l	Mixing length
l'	Mixing length at wall
M	$R\bar{W}$
m	$r\bar{W}$
p	Gauge pressure
Q	Volume flow rate
R	r/r_o
Re	Reynolds number $\rho Qr_o/\mu$
r	Radius
S_i	Swirl intensity
$\hat{S}_i$	Swirl intensity at inlet to test section
U	$\bar{U}/U_{av}$
$\bar{U}$	Time mean axial velocity
$\tilde{U}$	$\bar{U}+u'$
U_{av}	Q/A
u'	Fluctuating axial velocity
V	$\bar{V}/U_{av}$
$\bar{V}$	Time mean radial velocity
$\tilde{V}$	$\bar{V}+v'$
v'	Fluctuating radial velocity
W	$\bar{W}/U_{av}$
$\bar{W}$	Time mean tangential velocity
$\tilde{W}$	$\bar{W}+w'$
w'	Fluctuating tangential velocity
X	x/r_o
x	Axial distance measured from entry to test section
y	Distance measured normal to wall
α	Radius ratio $\equiv r_i/r_o$
ε	Dissipation rate of turbulence per unit mass
ζ	Vorticity
ζ'	$\zeta r_o/U_{av}$
θ	Angular coordinate in cylindrical system
μ	Dynamic viscosity
μ_e	Effective viscosity
μ_t	Turbulent viscosity
μ'_e	μ_e/μ
μ'_t	μ_t/μ
ρ	Density
$\sigma_{k,t}$	Prandtl number for turbulent kinetic energy
$\sigma_{\varepsilon t}$	Prandtl number for dissipation rate of turbulent energy
τ	Shear stress
τ'	Shear stress at wall
Φ	Function used in Eq (31) and defined in Table 3
ϕ	Function used in Eq (28) and defined in Table 2
ψ	Stream function
Ω	ζ'/R
ω	ζ/r

Subscripts

i	Inner
o	Outer
r	Radial direction
x	Axial direction
θ	Tangential direction

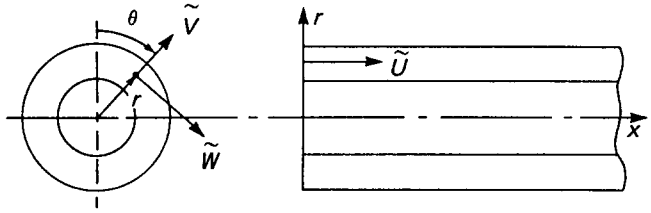

Fig 1 Coordinate system

With ρ representing the density of the fluid and μ its dynamic viscosity, the equations of continuity and the Navier–Stokes equations for a swirling fluid passing along the annulus, with the absence of body forces, may be written for the time average motion as

Continuity equation:

$$\frac{\partial}{\partial x}(r\bar{U})+\frac{\partial}{\partial r}(r\bar{V})=0 \tag{2}$$

Axial momentum equation:

$$\rho\left\{\bar{U}\frac{\partial\bar{U}}{\partial x}+\bar{V}\frac{\partial\bar{U}}{\partial r}\right\}=-\frac{\partial p}{\partial x}+\mu\nabla^2\bar{U}-\rho\left\{\frac{\partial\overline{u'^2}}{\partial x}+\frac{1}{r}\frac{\partial}{\partial r}(\overline{ru'v'})\right\} \tag{3}$$

Radial momentum equation:

$$\rho\left\{\bar{U}\frac{\partial\bar{V}}{\partial x}+\bar{V}\frac{\partial\bar{V}}{\partial r}-\frac{\bar{W}^2}{r}\right\}=-\frac{\partial p}{\partial r}+\mu\left\{\nabla^2\bar{V}-\frac{\bar{V}}{r^2}\right\}$$
$$-\rho\left\{\frac{\partial}{\partial x}(\overline{u'v'})+\frac{1}{r}\frac{\partial}{\partial r}(r\overline{v'^2})-\frac{\overline{W'^2}}{r}\right\} \tag{4}$$

Tangential momentum equation:

$$\rho\left\{\bar{U}\frac{\partial\bar{W}}{\partial x}+\bar{V}\frac{\partial\bar{W}}{\partial r}+\frac{\bar{W}\bar{V}}{r}\right\}\mu\left\{\nabla^2\bar{W}-\frac{\bar{W}}{r^2}\right\}$$
$$-\rho\left\{\frac{\partial}{\partial x}\left(\frac{r^2}{u'v'}\right)+\frac{\partial}{\partial r}(v'w')+2\frac{\overline{v'w'}}{r}\right\} \tag{5}$$

where

$$\nabla^2=\frac{\partial^2}{\partial x^2}+\frac{\partial^2}{\partial r^2}+\frac{1}{r}\frac{\partial}{\partial r}$$

and p represents the local pressure in the flow.

The time averages of the fluctuating velocity products may be identified as turbulence stress components which may be combined with the appropriate time average components. As a result, we may adopt the concept of an effective viscosity μ_e given by

$$\mu_e=\mu+\mu_t \tag{6}$$

where μ_t accounts for the turbulence stresses and is called turbulent viscosity. Under these circumstances Eqs (2) to (5) may be rewritten in the following form:

$$\frac{\partial\bar{U}}{\partial x}+\frac{\partial\bar{V}}{\partial r}+\frac{\bar{V}}{r}=0 \tag{7}$$

$$\rho\left\{\bar{U}\frac{\partial\bar{U}}{\partial x}+\bar{V}\frac{\partial\bar{U}}{\partial r}\right\}$$
$$=-\frac{\partial p}{\partial x}+\frac{1}{r}\frac{\partial}{\partial r}\left\{r\mu_e\left(\frac{\partial\bar{V}}{\partial x}+\frac{\partial\bar{U}}{\partial r}\right)\right\}+2\frac{\partial}{\partial x}\left(\mu_e\frac{\partial\bar{U}}{\partial x}\right) \tag{8}$$

$$\rho\left\{\bar{U}\frac{\partial\bar{V}}{\partial x}+\bar{V}\frac{\partial\bar{V}}{\partial r}-\frac{\bar{W}^2}{r}\right\}=-\frac{\partial p}{\partial r}+\frac{\partial}{\partial x}\left\{\mu_e\left(\frac{\partial\bar{V}}{\partial x}+\frac{\partial\bar{U}}{\partial r}\right)\right\}$$
$$+\frac{2}{r}\frac{\partial}{\partial r}\left\{r\mu_e\frac{\partial\bar{V}}{\partial r}\right\}-2\mu_e\frac{\bar{V}}{r^2} \tag{9}$$

$$\rho\left\{\bar{U}\frac{\partial\bar{W}}{\partial x}+\bar{V}\frac{\partial\bar{W}}{\partial r}+\frac{\bar{V}\bar{W}}{r}\right\}$$
$$=\frac{1}{r^2}\frac{\partial}{\partial r}\left\{r^3\mu_e\frac{\partial}{\partial r}\left(\frac{\bar{W}}{r}\right)\right\}+\frac{\partial}{\partial x}\left(\mu_e\frac{\partial\bar{W}}{\partial x}\right) \tag{10}$$

The four Eqs (7) to (10) can therefore be used to solve for the four field variables U, $\bar{V}$, $\bar{W}$ and p provided that some model for the spatial dependence of μ_e can be used. Although the matter is straightforward for laminar flow, for then $\mu_e=\mu$, which is a physical property of the fluid, the formulation of an accurate and plausible turbulence model to determine μ_e is difficult if some degree of general applicability is preserved.

Mathematical modelling of turbulence

Various proposals, referred to as 'turbulence models', for representing the turbulence stress tensor have been summarized by Rodi[14]. These are essentially models for μ_e, and some require the use of other differential transport equations whereas others involve algebraic relations. In this study, two models have been used, namely:

(a) the Prandtl mixing length hypothesis:
(b) the k–ε model, in which two differential equations are used to describe the turbulence kinetic energy per unit mass, k and the dissipation rate of turbulence energy per unit mass, ε.

In case (a) the turbulence viscosity is related to the appropriate mean strain rate by the so-called mixing length l, which is itself proportional to a characteristic length for the flow. Thus, taking the x-direction as an example,

$$\mu_{t,x}=\rho l_x^2\left|\frac{\partial\bar{U}}{\partial r}\right| \tag{11}$$

and so

$$\mu_{e,x}=\mu+\rho l_x^2\left|\frac{\partial\bar{U}}{\partial r}\right| \tag{12}$$

Similarly, for the tangential direction, we have

$$\mu_{e,\theta}=\mu+\rho l_\theta^2 r\left|\frac{\partial}{\partial r}\left(\frac{\bar{W}}{r}\right)\right| \tag{13}$$

Hence, from Eqs (12) and (13), and by analogy with Stokes's law for laminar flows, the total axial and shear stresses may be introduced, respectively, as

$$\tau_{r,x}=\mu_{e,x}\frac{\partial\bar{U}}{\partial r} \tag{14}$$

$$\tau_{r,\theta}=\mu_{e,\theta}r\frac{\partial}{\partial r}\left(\frac{\bar{W}}{r}\right) \tag{15}$$

It may be noted here that special consideration must be given to these expressions close to a solid wall, as is described below.

For complicated three-dimensional flows, especially swirling and separated flows, the governing equations of motion are elliptic, and hence convective transport of momentum may be significant. It is then more difficult to prescribe l algebraically, and thus mixing length models may lose accuracy. Although the two-equation k–ε model is by no means complete for flows described by elliptic equations, such a model does have the advantage that l can be calculated. Jones and Launder[15] were the forst to put forward a relatively simple k–ε model which was a special case, applicable to high Reynolds numbers, of the exact equation derived by Harlow and Nakayama[16]. Thus, for case (b) we adopt the Jones and Launder expression

$$\mu_t=C_\mu\rho k^2/\varepsilon \tag{16}$$

where C_μ is a constant. The corresponding (coupled) equations for k and ε are then, respectively,

$$\rho\left\{\bar{U}\frac{\partial k}{\partial x}+\bar{V}\frac{\partial k}{\partial r}\right\}=\frac{\partial}{\partial x}\left\{\frac{\mu_t}{\sigma_{k,t}}\frac{\partial k}{\partial x}\right\}+\frac{1}{r}\frac{\partial}{\partial r}\left\{\frac{\mu_t}{\sigma_{k,t}}r\frac{\partial k}{\partial r}\right\}-\rho\varepsilon+\mu_t G \tag{17}$$

$$\rho\left\{\bar{U}\frac{\partial \varepsilon}{\partial x}+\bar{V}\frac{\partial \varepsilon}{\partial r}\right\}=\frac{\partial}{\partial x}\left\{\frac{\mu_t}{\sigma_{\varepsilon,t}}\frac{\partial \varepsilon}{\partial x}\right\}+\frac{1}{r}\frac{\partial}{\partial r}\left\{\frac{\mu_t}{\sigma_{\varepsilon,t}}r\frac{\partial \varepsilon}{\partial r}\right\}+C_1\frac{\varepsilon}{k}\mu_t G-\rho C_2\frac{\varepsilon^2}{k} \tag{18}$$

where G is referred to as the generation term and is given by

$$G=2\left\{\left(\frac{\partial\bar{U}}{\partial x}\right)^2+\left(\frac{\partial\bar{V}}{\partial r}\right)^2+\left(\frac{\bar{V}}{r}\right)^2\right\}+\left\{\frac{\partial\bar{U}}{\partial r}+\frac{\partial\bar{V}}{\partial x}\right\}^2+\left(\frac{\partial\bar{W}}{\partial x}\right)^2+\left\{\frac{\partial\bar{W}}{\partial r}-\frac{\bar{W}}{r}\right\}^2 \tag{19}$$

and $\sigma_{k,t}$ is the Prandtl number for turbulent kinetic energy, $\sigma_{\varepsilon,t}$ the Prandtl number for dissipation rate of turbulent energy, and C_1 and C_2 are constants.

An examination of previous work and a series of computer analyses by the present authors has led to the adoption of numerical values of the constants C_μ, $\sigma_{k,t}$, $\sigma_{\varepsilon,t}$, C_1, C_2 as shown in Table 1.

Transformation of the equations of motion

The governing equations of motion (7) to (10) are seen to be elliptic and so require boundary conditions for each equation on all boundaries. A finite difference technique is used which is an adaptation of the approach developed by Gosman *et al*[10]. In this, the primitive variables $\bar{U}$ and $\bar{V}$ are replaced in non-swirling flow by vorticity ζ and stream function ψ, and p may be eliminated by cross-differentiation. When swirl is present we retain ζ and ψ of the previous axial flow and introduce the additional term $m\equiv r\bar{W}$, which represents the angular momentum per unit mass about the x axis in Fig 1. Thus the vorticity in the x–r plane may be expressed as

$$\zeta=\frac{\partial\bar{V}}{\partial x}-\frac{\partial\bar{U}}{\partial r} \tag{20}$$

and the stream function satisfies the relations

$$\psi=\int r\bar{U}\,dr=-\int r\bar{V}\,dx \tag{21}$$

whence

$$\bar{U}=\frac{1}{r}\frac{\partial\psi}{\partial r}\qquad \bar{V}=-\frac{1}{r}\frac{\partial\psi}{\partial x} \tag{22}$$

and it is seen that ψ satisfies the continuity equation (7), as it should by definition. The vorticity may also be written in terms of stream function as follows

$$\zeta=\frac{1}{r}\frac{\partial^2\psi}{\partial r^2}-\frac{1}{r}\frac{\partial^2\psi}{\partial x^2}-\frac{\bar{U}}{r} \tag{23}$$

Now, if Eq (8) is differentiated with respect to r, and Eq (9) differentiated with respect to x, the term $-\partial^2 p/\partial x\partial r$ may be eliminated from the resulting equations. The vorticity and stream function can then be introduced into the resulting equation to give the so called 'vorticity' equation,

$$\rho r^2\left\{\frac{\partial}{\partial x}\left(\frac{\zeta}{r}\frac{\partial\psi}{\partial r}\right)-\frac{\partial}{\partial r}\left(\frac{\zeta}{r}\frac{\partial\psi}{\partial x}\right)\right\}-\frac{\partial}{\partial x}\left\{r^3\frac{\partial}{\partial x}\left(\mu_e\frac{\zeta}{r}\right)\right\}-\frac{\partial}{\partial r}\left\{r^3\frac{\partial}{\partial r}\left(\mu_e\frac{\zeta}{r}\right)\right\}-\rho r\frac{\partial}{\partial x}(\bar{W}^2)-F_\mu=0 \tag{24}$$

The function F_μ is given by

$$F_\mu=2r^2\left[\frac{\partial^2}{\partial x^2}\left(\mu_e\frac{\partial\bar{U}}{\partial r}\right)-\frac{\partial^2}{\partial r^2}\left(\mu_e\frac{\partial\bar{V}}{\partial x}\right)+\frac{\partial^2}{\partial x\partial r}\times\left\{\mu_e\left(\frac{\partial\bar{V}}{\partial r}-\frac{\partial\bar{U}}{\partial x}\right)\right\}+\frac{1}{r}\frac{\partial}{\partial x}\left(\mu_e\frac{\partial\bar{V}}{\partial r}\right)-\frac{1}{r}\frac{\partial}{\partial r}\left(\mu_e\frac{\partial\bar{V}}{\partial x}\right)-\frac{\bar{V}}{r^2}\frac{\partial\mu_e}{\partial x}\right] \tag{25}$$

It has been argued by Gosman *et al*[10], Crane and Burley[11], Okhio[17] and others that F_μ is negligibly small, and evidence from jet flows certainly supports this assumption. However, no such evidence is available from

Table 1 Empirical constants used in k–ε model

Source	C_μ	$\sigma_{k,t}$	$\sigma_{\varepsilon,t}$	C_1	C_2
Kubo and Gouldin[11]	0.09	1.0	1.3	1.40	1.95
Jones and Launder[15]	0.09	1.0	1.3	1.55	2.00
Hanjalic and Launder[23]	0.07	1.0	1.1	1.45	2.00
Present	0.08	1.0	1.3	1.50	1.98

Table 2 Dimensional functions in Eq (28)

ϕ	a_ϕ	b_ϕ	c_ϕ	d_ϕ
$\omega \equiv \zeta/r$	ρr^2	r^2	μ_e	$-\frac{1}{r}\left\{\frac{\rho}{r}\frac{\partial(m^2)}{\partial x}+F_\mu\right\}$
ψ	0	$1/r^2$	1	$-\omega$
$m=r\bar{W}$	ρ	r^2/μ_e	$1/r^2$	0
k	ρ	$\mu_t/\sigma_{k,t}$	1	$\rho\varepsilon-\mu_t G$
ε	ρ	$\mu_t/\sigma_{\varepsilon,t}$	1	$-\frac{\varepsilon}{K}\left\{C_1\mu_t G-\rho C_2\varepsilon\right\}$

annulus flows, and thus this function is retained in the numerical analysis.

The 'stream function' equation may be formed from Eqs (20) and (22):

$$\frac{\partial}{\partial x}\left(\frac{1}{r}\frac{\partial\psi}{\partial x}\right)+\frac{\partial}{\partial r}\left(\frac{1}{r}\frac{\partial\psi}{\partial r}\right)+\zeta=0 \tag{26}$$

The third equation necessary for a complete solution may be obtained from Eq (10), on substitution for $\bar{U}$ and $\bar{V}$ from Eq (22), to give the 'swirl' equation

$$\rho\left\{\frac{\partial}{\partial x}\left(r\bar{W}\frac{\partial\psi}{\partial r}\right)-\frac{\partial}{\partial r}\left(r\bar{W}\frac{\partial\psi}{\partial x}\right)\right\} -\frac{\partial}{\partial x}\left\{r^3\mu_e\frac{\partial}{\partial x}\left(\frac{\bar{W}}{r}\right)\right\}-\frac{\partial}{\partial r}\left\{r^3\mu_e\frac{\partial}{\partial r}\left(\frac{\bar{W}}{r}\right)\right\}=0 \tag{27}$$

The variable $\omega=\zeta/r$ is now introduced and may be used with m, already defined, and ψ to provide a general equation for the purposes of computer solution. Reference to Eqs (24), (26) and (27) and also to the k–ε Eqs (17) and (18) shows that all may be represented by the following general equation applicable to axisymmetric swirling flows:

$$a_\phi\left\{\frac{\partial}{\partial x}\left(\phi\frac{\partial\psi}{\partial r}\right)-\frac{\partial}{\partial r}\left(\phi\frac{\partial\psi}{\partial x}\right)\right\}-\frac{\partial}{\partial x}\left\{b_\phi r\frac{\partial}{\partial x}(c_\phi\phi)\right\} -\frac{\partial}{\partial r}\left\{b_\phi r\frac{\partial}{\partial r}(c_\phi\phi)\right\}+rd_\phi=0 \tag{28}$$

The functions a_ϕ, b_ϕ, c_ϕ and d_ϕ in Eq (28), related to each independent variable ϕ, are given in Table 2. We see, therefore, that the same technique for the solution of Eq (28) for one ϕ can be used throughout. It may also be noted that the coefficients in Table 2 apply for both laminar and turbulent flows. In the case of laminar flow, it is more convenient to derive dimensionless forms of Eqs (24), (26) and (27). The following substitutions are therefore used:

$$\begin{aligned}
&R=r/r_o && X=x/r_o\\
&W=\bar{W}/U_{av} && \zeta'=\zeta r_o/U_{av}\\
&\mu_e'=\mu_e/\mu && \mu_t'=\mu_t/\mu\\
&F_\mu'=r_o F_\mu/\mu U_{av}\\
&U=\bar{U}/U_{av} && V=\bar{V}/U_{av}\\
&\Omega=\zeta'/R && \Psi=\psi/U_{av}r_o^2\\
&Re=\rho U_{av}r_o/\mu && M=RW
\end{aligned} \tag{29}$$

The average velocity U_{av} is defined as the volume flow rate of fluid passing through the annulus divided by the annulus cross-sectional area perpendicular to the flow direction. We can therefore write

$$U_{av}=\frac{Q}{A}=\frac{\int_{r_i}^{r_o}2\pi r\bar{U}\,dr}{\pi(r_o^2-r_i^2)} \tag{30}$$

The transformed equations of motion may still be arranged in the form of Eq (28), but in dimensionless terms, ie

$$A_\Phi\left\{\frac{\partial}{\partial x}\left(\Phi\frac{\partial\Psi}{\partial R}\right)-\frac{\partial}{\partial R}\left(\Phi\frac{\partial\Psi}{\partial X}\right)\right\}-\frac{\partial}{\partial X}\left\{B_\Phi R\frac{\partial}{\partial X}(C_\Phi\Phi)\right\} -\frac{\partial}{\partial R}\left\{B_\Phi R\frac{\partial}{\partial R}(C_\Phi\Phi)\right\}+RD_\Phi=0 \tag{31}$$

The functions A_Φ, B_Φ, C_Φ, D_Φ for appropriate interpretations of Φ are shown in Table 3. Using the data of Tables 2 and 3 Eqs (28) and (31) can be converted to a finite difference form.

The technique employed is an adaptation of the relaxation method developed by Gosman *et al*[10]. A detailed description of the problem in hand can be found elsewhere[4].

Boundary conditions

In order to obtain a solution of the general elliptic partial differential Eq (28) or the dimensionless form, Eq (31), boundary conditions must be specified at all points on the boundaries enclosing the field of flow. These boundaries are at inner and outer walls and at the entrance to an exit from the annular test section. Clearly, for the analytical predictions to resemble accurately the measured flow field, the boundary conditions must reflect experimental conditions as closely as possible. A problem is therefore immediately posed by the exit condition, for we suppose the test section to be sufficiently long for the swirl velocity to decay asymptotically to zero. Although this exit condition will applied in a numerical solution, consistent with a specified accuracy in the prediction of velocity components, the extent of an experimental test section is unlikely to satisfy the same requirements. We can, nevertheless, examine the experimental development of flow for a given test section and make comparisons with corresponding data from numerical predictions within the same test section length. Finally, it may be noted that a theoretical prediction of the flow field obtained independently of all empiricism cannot yet be obtained. Consequently, some boundary conditions are formulated with the aid of experimental data[1,2], although such dependence is intentionally kept to a minimum.

The boundary conditions adopted are briefly summarized below.

Table 3 Dimensionless functions in Eq (31)

Φ	A_Φ	B_Φ	C_Φ	D_Φ
Ω	R^2Re	R^2	μ_e^1	$-\frac{1}{R}\left\{\frac{Re}{R}\frac{\partial(M^2)}{\partial X}+F_\mu^1\right\}$
Ψ	0	$1/R^2$	1	$-\Omega$
M	Re	$R^2\mu_e^1$	$1/R^2$	0

Conditions at inlet

Vorticity

The vorticity distribution at inlet may be estimated from Eq (20), in which the component velocity gradients are assumed to be known experimentally or specified mathematically. In particular, for the data of Ref 1, against which the present predictions are to be tested, the axial velocity is uniform at entry and no radial velocity exists there. Hence we may write

$$\zeta(r,\mathrm{o})=0=\Omega(R,\mathrm{o}) \tag{32}$$

Stream function

The first of Eqs (21) may be used to determine the radial variation of stream function, that is

$$\psi(r,\mathrm{o})=\int_{r_\mathrm{i}}^{r} r\bar{U}\,\mathrm{d}r=\frac{1}{2}\bar{U}(r^2-r_\mathrm{i}^2) \tag{33a}$$

for uniform axial velocity at entry. Similarly, in dimensionless form,

$$\Psi(R,\mathrm{o})=\frac{1}{2}U(R^2-\alpha^2) \tag{33b}$$

where the annulus radius ratio $\alpha=r_\mathrm{i}/r_\mathrm{o}$. It may also be noted that for uniform axial velocity at entry, Eq (30) shows that

$$U_\mathrm{av}=\bar{U}(R,\mathrm{o})$$

whence Eq (33b) reduces to

$$\Psi(R,\mathrm{o})=\frac{1}{2}(R^2-\alpha^2) \tag{34}$$

Angular momentum

Since the flow at inlet is considered specified, then $m(r,\mathrm{o})$ and hence $M(R,\mathrm{o})$ are presumed known. In the experimental work described in Ref 1 the boundary layers which developed on the walls of the conditioning section were removed by suction. Thus flow at inlet to the test section could be considered inviscid since tangential velocity gradients were absent. One may thus contemplate a variety of angular momentum distributions depending on the technique used for introducing swirl to the flow. In the authors' experiments a free vortex, ie constant angular momentum, was chosen as the inlet conditions although some workers have examined forced vortex conditions. Only with suction facilities can close simulation of the inviscid conditions be obtained, however, and the closeness to free vortex flow can be seen in Ref 1. For the sake of ease in calculations, a least-squares fit can be used to obtain the 'nominal' free vortex relation from the measured data. In general, of course, the momentum equations can be satisfied point-by-point across the inlet plane.

Mixing length hypothesis

A detailed examination of the experimental data obtained from swirling flows in annuli[1,2] revealed that $\mu_{t,x}$ had a value of 2.0 to good accuracy. The value of $\mu_{t,\theta}$ was estimated from the same source of data using the expression

$$\mu_{t,\theta}=\rho\overline{v'w'}\Big/\left(\frac{\partial\bar{W}}{\partial r}-\frac{\bar{W}}{r}\right) \tag{35}$$

Model for k and ε

Experimental data from Ref 1 were used with Eqs (17), (18), (19) and the constants shown in Table 1 to calculate values of k and ε at the inlet plane. Should such data not be available then the Gosman and Pun[18] formula may be used:

$$k=0.035\bar{U}^2 \tag{36}$$

The energy dissipation rate is not usually known and so it is calculated from the viscosity relation, Eq (16). If available, μ_t can be deduced from turbulences stress data, as herein, or from mixing length theory.

Conditions near the walls

Vorticity

There is some difficulty in obtaining the vorticity conditions close to walls, and care must be exercised in handling them. Indeed, mathematical divergence and instability may occur if the wrong boundary conditions are used. In this study two different techniques of approximating the vorticity at solid walls are employed.

The first method makes use of the vorticity Eq (24) to obtain $\omega=\zeta/r$, but the following assumptions have to be made:

(a) the longitudinal gradient of ω is negligible compared with the radial gradient of ω;
(b) the walls are impermeable and no slip takes place there;
(c) $M\rightarrow 0$, $\partial\psi/\partial x\rightarrow 0$ and μ_e is constant.

Eq (24) then reduces to

$$\mu_\mathrm{e}\frac{\partial}{\partial r}\left(r^3\frac{\partial\omega}{\partial r}\right)=0$$

which may be integrated twice with respect to r between r_i and r to give

$$\omega-\omega_\mathrm{i}=\frac{C_3}{2}\left[\frac{1}{r_\mathrm{i}^2}-\frac{1}{r^2}\right]$$

where

$$C_3=r^3\frac{\partial\omega}{\partial r}$$

is a constant. Substitution for ω into Eq (26) applied close to a wall and then integrating twice with respect to r gives the following expression for regions of the flow field very close to the inner wall:

$$\psi-\psi_\mathrm{i}=\frac{C_3}{2}\left\{\frac{r^2}{2}\ln\left(\frac{r}{r_\mathrm{i}}\right)-\frac{1}{4}(r^2-r_\mathrm{i}^2)\right\}-\left\{\omega_\mathrm{i}+\frac{C_3}{2r_\mathrm{i}^2}\right\}\frac{(r^2-r_\mathrm{i}^2)^2}{8} \tag{37}$$

and in this region $\ln(r/r_\mathrm{i})$ tends to zero so that

$$\psi-\psi_\mathrm{i}=-\omega_\mathrm{i}\frac{(r^2-r_\mathrm{i}^2)^2}{8}-\frac{C_3}{16r_\mathrm{i}^2}(r^4-r_\mathrm{i}^4) \tag{38}$$

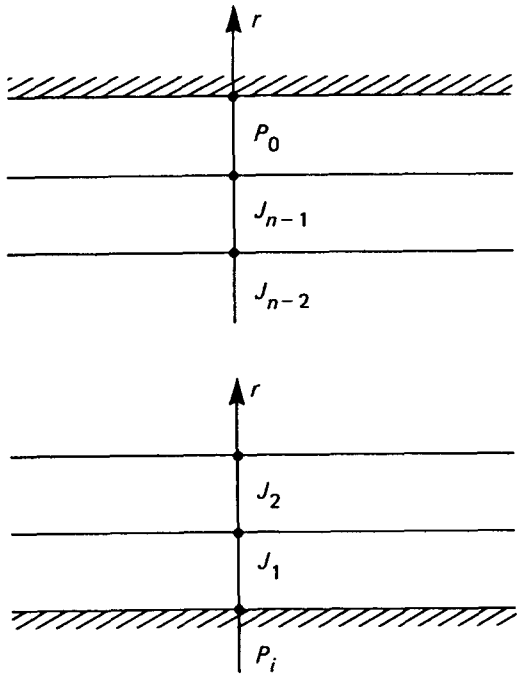

Fig 2 Grid points for flow near to walls

The vorticity at the inner wall is $(r\omega)_i = \zeta_i$ and

$$\frac{\partial \zeta}{\partial r} = \frac{\partial (r\omega)}{\partial r} = r\frac{\partial \omega}{\partial r} + \omega = \frac{C_3}{r^2} + \omega_i$$

and so at the inner wall

$$r_i\omega_i = \frac{r_i[16(\psi - \psi_i) + (r^4 - r_i^4)\{\partial(r\omega)/\partial r\}_i]}{(4r^2r_i^2 - 3r_i^4 - r^4)} \tag{39a}$$

or, in dimensionless form,

$$\alpha\Omega_i = \frac{\alpha[16(\Psi - \Psi_i) + (R^4 - \alpha^4)\{\partial(R\Omega)/\partial R\}_i]}{(4R^2\alpha^2 - 3\alpha^4 - R^4)} \tag{39b}$$

Thus, it can be seen that the vorticity at the inner wall can be expressed in terms of the stream function and vorticity at points close to the wall since the derivative can be evaluated in terms of a Taylor expansion. Similar development allows the determination of the vorticity at the outlet wall following integration over the range $r \rightarrow r_o$.

In the second method the stream function Eq (26) is approximated for conditions close to a wall, ie with $\partial\psi/\partial x = 0$ and r constant, to give

$$\zeta = r\omega = -\frac{1}{r}\frac{\partial^2\psi}{\partial r^2}$$

to give vorticity in terms of stream function close to solid walls. The second derivative of ψ can be deduced from a Taylor expansion to second order using the definitions in Fig 2 to estimate ω.

For the inner wall at point P_i

$$\omega_{P_i} = -\frac{2}{r_{P_i}^2}\left\{\frac{r_{J_2}^3\psi_{J_1} - r_{J_1}^3\psi_{J_2}}{r_{J_2}^3 r_{J_1}^2 - r_{J_1}^3 r_{J_2}^2}\right\} \tag{40a}$$

that is

$$\Omega_{P_i} = -\frac{2}{\alpha^2}\left\{\frac{R_{J_2}^3\Psi_{J_1} - R_{J_1}^3\Psi_{J_2}}{R_{J_2}^3 R_{J_1} - R_{J_1}^3 R_{J_2}^2}\right\} \tag{40b}$$

For the outer wall at point P_o

$$\omega_{P_o} = -\frac{2}{r_{P_o}^2}\left\{\frac{r_{J_{n-2}}^3(\psi_{J_{n-1}} - \psi_{P_o}) - r_{J_{n-1}}^3(\psi_{J_{n-2}} - \psi_{P_o})}{r_{J_{n-2}}^3 r_{J_{n-1}}^2 - r_{J_{n-1}}^3 r_{J_{n-2}}^2}\right\} \tag{41a}$$

that is

$$\Omega_{P_o} = -2\left\{\frac{R_{J_{n-2}}^3(\Psi_{J_{n-1}} - \Psi_{P_o}) - R_{J_{n-1}}^3(\Psi_{J_{n-2}} - \Psi_{P_o})}{R_{J_{n-2}}^3 R_{J_{n-1}}^2 - R_{J_{n-1}}^3 R_{J_{n-2}}^2}\right\} \tag{41b}$$

Stream function

As a result of impermeability and no slip at the walls there can be no velocity component there. Thus ψ must be constant on the walls. Without loss of generality we may take $\psi(r_i, x) = 0 = \Psi(\alpha, X)$ and

$$\psi(r_o, x) = \int_{r_i}^{r_o} r\bar{U}\,dr \tag{42a}$$

that is

$$\Psi(1, X) = \int_{\alpha}^{1} RU\,dR \tag{42b}$$

Angular momentum

Since the inner and outer walls are both stationary and as there is no slip on the walls,

$$m(r_i, x) = 0 = m(r_o, x) \tag{43a}$$

that is

$$M(\alpha, X) = 0 = M(1, X) \tag{43b}$$

Mixing length hypothesis

Close to a wall the dynamic viscosity μ plays an important role and so using the Van Driest proposal[19] with the modified version of shear stress developed by Patankar and Spalding[7] the following relationsships for mixing length were used:

$$l'_{x \text{ or } \theta} = Ky\left[1 - \exp\left\{-\frac{y(\rho\tau'_{x \text{ or } \theta})^{1/2}}{A'\mu}\right\}\right] \tag{44}$$

where the prime denotes values taken at the walls, and y is the distance from the wall. The numerical values of the constants that were used are $K = 0.4$ and $A' = 26.0$. In the present work it was found to be sufficiently accurate to take $l'_x = l'_\theta$ and so μ_e could be estimated near to the inner and outer walls.

Model for k and ε

Use is made of the well-known 'wall functions', which are algebraic relations based on the logarithmic law of the wall, to estimate k and ε at the walls. The expressions adopted in the analysis are as follows:

$$k_P = \frac{\tau_r/\rho}{(C_\mu C_D)^{1/2}} \tag{45}$$

$$\varepsilon_P = \frac{(\tau_r/\rho)^{3/2}}{K_C y_P} \tag{46}$$

where τ_r represents the resultant shear stress a short distance y_P from the wall point P. The constants C_μ, C_D and K_C are taken to be 0.09, 0.075 and 0.418 respectively. Values of k_P and ε_P so deduced are considered to apply at the walls, and further details are given by Morsi[4].

Conditions at outlet

It was found from computational experiments with simpler analyses on similar geometries that good agreement with experimentally measured data could be obtained with the following conditions applied at large distances from inlet:

$$\frac{\partial \phi}{\partial x}=0=\frac{\partial \Phi}{\partial X} \tag{47}$$

and

$$\frac{\partial^2 \phi}{\partial x^2}=0=\frac{\partial^2 \Phi}{\partial X^2} \tag{48}$$

where ϕ and Φ take on the parameters shown in Tables 2 and 3.

Notes on computational procedure

The main details and a computer listing of all programs and subroutines are given in Ref 4. Here we are content to point out a number of important features which it is necessary to cover if a satisfactory set of calculations is to be produced.

A particularly important factor concerns the grid geometry to be employed in a finite difference solution of the elliptic equations (28) and (31) and their associated boundary conditions. In this study a non-uniform grid was used. This allows the adoption of fine mesh spacings in areas where spatial gradients are large, eg near the walls where boundary layer behaviour is important, and coarser spacings in other parts of the flow field, especially with increasing distance downstream from the inlet of the annular test section. It is then possible to make more efficient use of computer time and core store than if a uniform mesh size were used to give equivalent accuracy in regions of rapidly changing flow parameters. Unfortunately, the complexity of the resulting finite difference equations is greatly increased and care must also be taken in the construction of the mesh. The ratio of successive mesh spacings should not be made too different from unity and in the present work this ratio varied from 1.05 in regions close to the walls and annulus inlet to 1.25 towards the centre of the flow passage. Further discussion of these points may be found in Ref 10.

The non-linear nature of the equations of motion, combined with a strong coupling between them, may give rise to numerical instabilities leading to divergence of the solution during computations. In order to minimize the occurrence of unstable behaviour, the initial conditions for the first set of iterations were chosen such that the mean velocity satisfied continuity, and k and ε were based on estimates from values of shear stress and mixing length. To solve the equivalent finite difference equations, and obtain a converged solution, an iteration procedure using an under-relaxation technique was adopted, so that, for example,

$$\phi^n=\phi^{n-1}+f(\phi^n-\phi^{n-1}) \tag{49}$$

where the superscripts n and $n-1$ denote the number of iterations, ie ϕ^n is the solution of the nth iteration, and f is the under-relaxation factor, which had a value between 0.1 and 1.0.

Evidently, the rate of convergence of the procedure depends strongly on f, and for linear equations an optimum value of f which provides convergence rates that are an order of magnitude faster than the Gauss–Seidel scheme ($f=1.0$) is known to exist. Furthermore, simple linear equations are amenable to exact analytical treatment to derive the optimum relaxation parameters. No such results are available to determine the optimum relaxation parameter for the type of equation considered in this study. Thus one is forced to adopt a scanning procedure in which f is varied over a range, and the value selected which gives rise to the fewest number of iterations. The scanning was accomplished by first assuming f_ξ, for vorticity, was constant and then varying f_ψ, for stream function, to give best results; that is, with minimum number of iterations. The reverse procedure was then applied by keeping the 'best' f_ψ constant and determining f_ξ. With these values of f, one can estimate f_M, for 'angular momentum'. Typical values of under-relaxation factors obtained were $f_\psi=08$–09, $f_\xi=0.42$–0.45, $f_M=0.62$–0.7, $f_k=0.4$–0.45, $f_\varepsilon=0.42$–0.45.

To test the convergency of the solution of a particular variable Φ the convergency criterion used was

$$\{(\Phi^n-\Phi^{n-1})/\Phi^n\}_{\max}\leqslant CC \tag{50}$$

where CC had a typical value between 0.001 and 0.005.

Results

It is evident from the foregoing theoretical models that the success of predicting swirling flow behaviour in an internal system relies on the consistent combination of accurate equations of motion and boundary conditions, a plausible (and if possible general) turbulence model, and an accurate, stable numerical analysis. To test the efficiency of the present techniques in all these respects we concentrate primarily on the determination of various velocity profiles in relation to corresponding measurements. The equations governing the turbulent swirling flow under consideration are sufficiently general to include certain distinct problems as special cases. For example, swirling laminar flows are immediately treated by setting μ_e equal to (constant) μ, and pipe flow is obtained when $r_i=0=\alpha$ and the inner boundary conditions are modified to account for the absence of a centre body and the no-slip condition there so that $\psi=0$ and $\partial\zeta/\partial r=0$ on the pipe axis. Following the formulation of the complete computer program it seemed prudent to check its accuracy in solving some simpler problems for which other theoretical and/or experimental data were available for comparison. This was done for the following cases:

(a) laminar pipe flow;
(b) turbulent pipe flow, using both the previously discussed turbulence models;
(c) laminar annulus flow.

The present computer predictions for case (a) in which $W=0$ are shown in Fig 3 for the distribution of axial velocity $U=\bar{U}/U_{av}$. The experimental data are those of Nikuradse given, for example, by Goldstein[20]. Fig 3

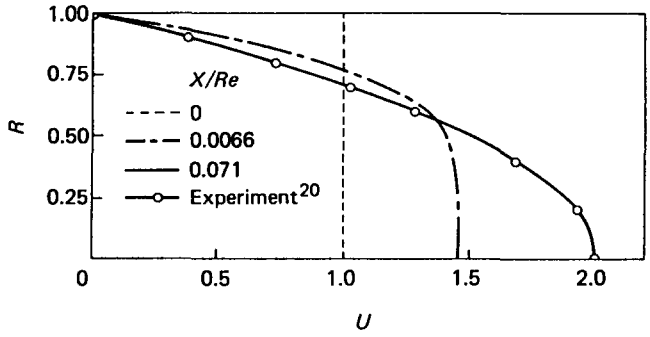

Fig 3 Development of laminar axial flow in a smooth pipe of circular cross-section

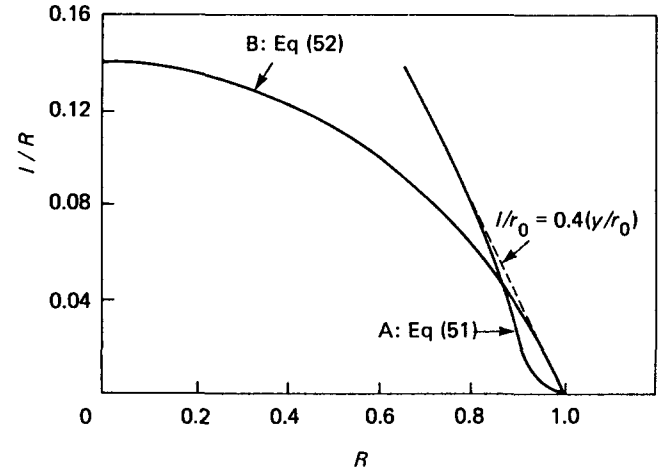

Fig 4 Radial distributions of mixing length in a circular-section pipe

illustrates the initial and fully developed velocity profile along with an intermediate stage. The fully developed condition is reached at $X/Re=0.071$, in agreement with Nikuradse's measurements and simplified theory.

Two turbulence models were examined for accuracy in case (b) where non-swirling pipe flows were considered for the sake of simplicity. In order to utilize the MLH model the distribution of mixing length l across the pipe was required, and so the data illustrated by curves A and B in Fig 4 were adopted. Curve A is applicable in the wall region and represents the Patankar–Spalding[7] modification of the Van Driest formula given by Eq (44), with $K=0.4$, $A=26.0$:

$$l=0.4y[1-\exp\{-y(\rho\tau)^{1/2}/26\mu\}] \qquad (51)$$

The value of the local shear stress was calculated from the logarithmic law of the wall. Curve B represents Nikuradse's formula, based on experimental data, which takes the form

$$l/r_o=0.14-0.08R^2-0.06R^4 \qquad (52)$$

Comparison is again made with Nikuradse's measurements (see Schlichting[21]) for turbulent flow in smooth pipes, and Fig 5 shows the fully developed axial velocity profiles for two Reynolds numbers. Excellent predictions from theory are again achieved. The flow becomes fully developed at $X=70$ for $Re=1.1\times10^5$ and $X=40$ for $Re=2\times10^6$.

The second turbulence model used was the k–ε formulation put forward by Jones and Launder[15] as discussed above. Eqs (17) and (18) were cast into finite difference form and the computer program modified accordingly. The value of μ_e was calculated from the sum of μ and μ_t given by Eq (16). The values of k and ε at the walls were derived on the basis of a Couette flow analysis using a wall flux relationship ('wall functions') as discussed earlier.

A converged solution, with $CC<0.001$, was obtained, from which it was observed that fully developed flow occurred at a distance $X=53$ for $Re=10^6$. This is again in agreement with Nikuradse's measurements of $X=50$ to 80 for a wide range of Reynolds numbers related to turbulent inlet flow to a circular section pipe.

Following these pipe investigations it was necessary to examine the calculation procedure for the annulus flows of the present geometry. Before a full consideration of turbulent flows was undertaken, the uncertainties associated with turbulence modesl were removed by adopting a constant molecular viscosity μ, and so an annular, laminar swirling flow was analysed. The initial swirl at inlet was considered to be free vortex with a variation given by

$$\bar{W}/U_{av}=W=r_o/r=R^{-1}$$

with a uniform axial velocity ($\bar{U}/U_{av}=U=1.0$) at inlet. This case was examined by Scott and Rask[9] but they used a radius ratio $\alpha=0.4$ whereas we use $\alpha=0.51$ here. However, before calculations were carried out the effects of two important factors, wall vorticity and effective viscosity function F_μ, were investigated.

The influence of wall vorticity boundary conditions on the rate of convergence and the accuracy of the results was considered necessary in view of the subsequent extensive computations. A comparative study

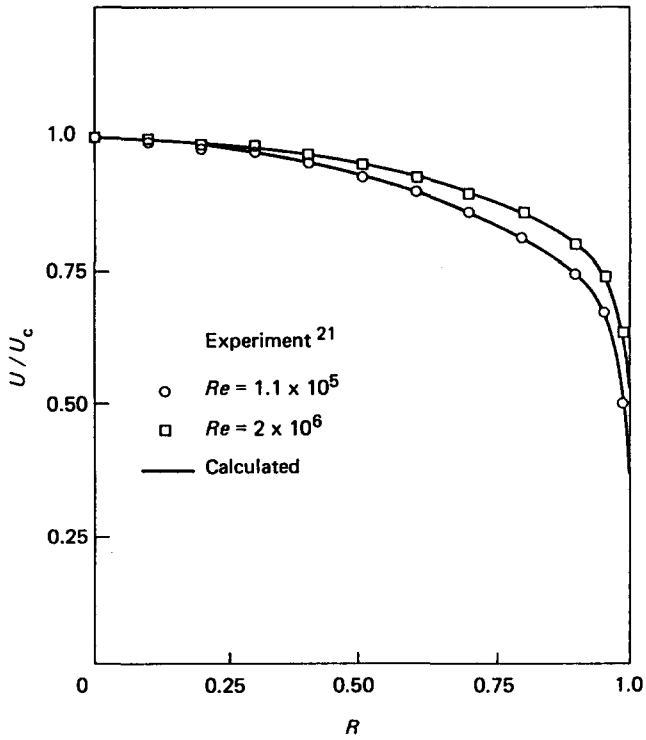

Fig 5 Fully developed axial velocity profiles for turbulent flow in a circular-section pipe; $\bar{U}_c$ is centreline velocity

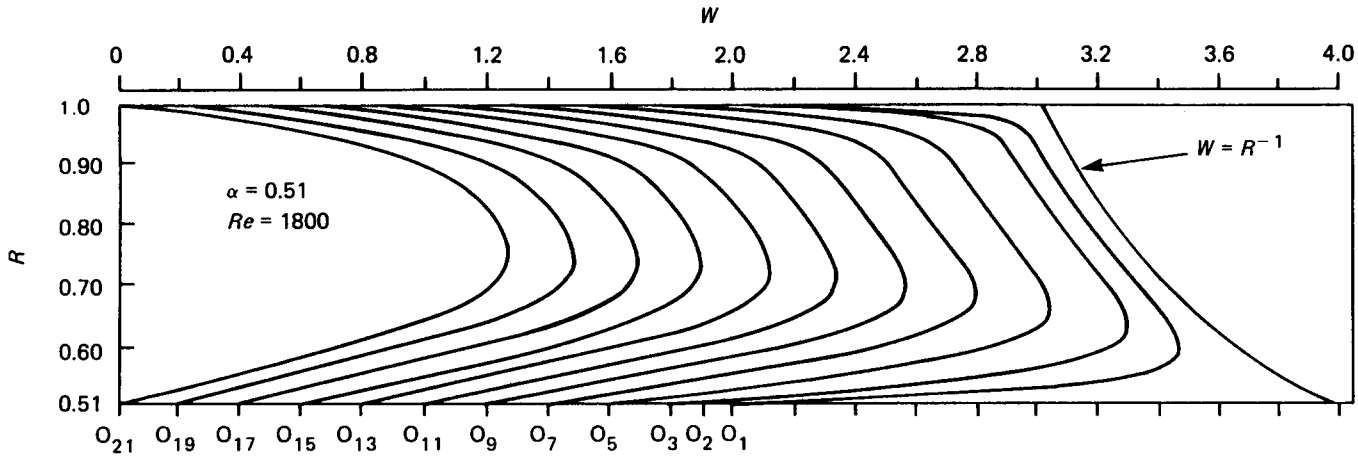

Fig 6 Predicted tangential velocity distribution across annulus for laminar flow and free vortex swirl distribution at inlet

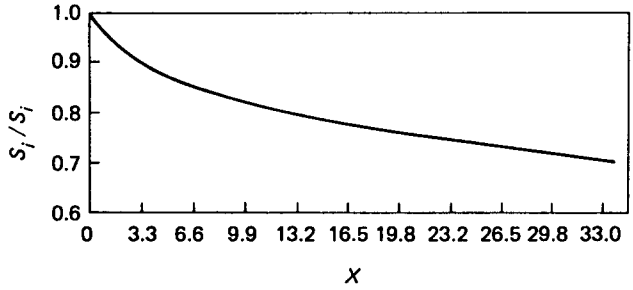

Fig 7 Predicted decay of swirl intensity along annulus for laminar velocity profiles and flow conditions shown in Fig 6

was made of the two different formulations for the wall vorticity, leading to Eqs (39a) and (41b). Test computer runs, with identical input data, for each of these formulations, produced results in very close agreement. However, the condition (39a) was found to give a somewhat faster rate of convergence for the vorticity cycle, and so it was used throughout succeeding calculations.

Initially, all the terms for F_μ in Eq (25) were retained in computations. Subsequently, all terms associated with the radial velocity V were neglected, since experimental evidence has shown this velocity component to be small everywhere; even near the inlet it is far smaller than the other velocity components. Negligible difference in the predictions of velocity variations was observed. However, when the term

$$\frac{\partial^2}{\partial x^2}\left(\mu_e \frac{\partial \bar{U}}{\partial r}\right)$$

was neglected, a somewhat disordered axial velocity profile occurred near the walls, an unsurprising feature since $\partial \bar{U}/\partial r$ is significant there. Consequently, this term was retained throughout subsequent analyses.

Fig 6 shows the predicted tangential velocity profiles for laminar swirling flow in an annulus with free vortex swirl distribution and uniform axial velocity at inlet. It may be noted that the peak value of W migrates from the inner (convex) wall to the mid-annulus location with increasing distance along the annulus. Station 1 refers to inlet and the remaining stations to 21 are at equal intervals of $X = 1.65$. A measure of the rate at which the swirl momentum decays can be obtained from the swirl intensity S_i defined as the ratio of the total angular momentum at a particular station to the total axial momentum. Thus, in dimensionless form,

$$S_i = \int_\alpha^1 UWR^2\,dR \Big/ \int_\alpha^1 U^2 R\,dR \tag{53}$$

Fig 7 shows the variation of S_i as a proportion of the inlet value $\hat{S}_i$ for the velocity profiles of Fig 6. Following an initial rapid decay a region of exponential decay to $S_i = 0$ at $X = \infty$ takes place, although in the region $X = 16.5$ to 33.0 the variation is almost linear. Comparison with the swirl decay curves given by Clayton and Morsi[1], deduced from turbulent flow measurements, indicates a much slower rate of decay for laminar flow. This is primarily the result of turbulent viscosity, μ_t being much greater than molecular viscosity μ.

The complete computer program was set to solve turbulent swirling flow developing along an annulus and, for the calculations presented here, inlet conditions for all dependent variables were taken from experimental data along with the boundary conditions discussed earlier. In the first set of computer runs isotropic turbulence was assumed, ie $\mu_{e,x} = \mu_{e,\theta}$. Furthermore, a constant effective viscosity was adopted with ε deduced from the empirical relationship

$$\varepsilon = 0.404 Re^{0.305} \tag{54}$$

where the numerical constants were obtained from a comparison of experiment and predictions by the present authors and others. Although Eq (54) implies the unlikely event that ε depends only on Re, and is independent of x and r, it was found previously by Huang and Tsou[13] that such an assumption for turbulent free-swirling flow in a pipe yielded good agreement between theory and their experimental results. The present authors were somewhat surprised to find that when theoretical predictions were compared with experiment a better agreement occurred than that reported earlier by Yamamoto and Millar[8], especially in respect of the tangential velocity. In Ref 8, solutions were given for the parabolized Navier–Stokes equations, in which the second-order derivatives of the viscous terms for the axial direction were omitted from the momentum equations, in conjunction with a k–ε model. The present authors found, however, that the prediction

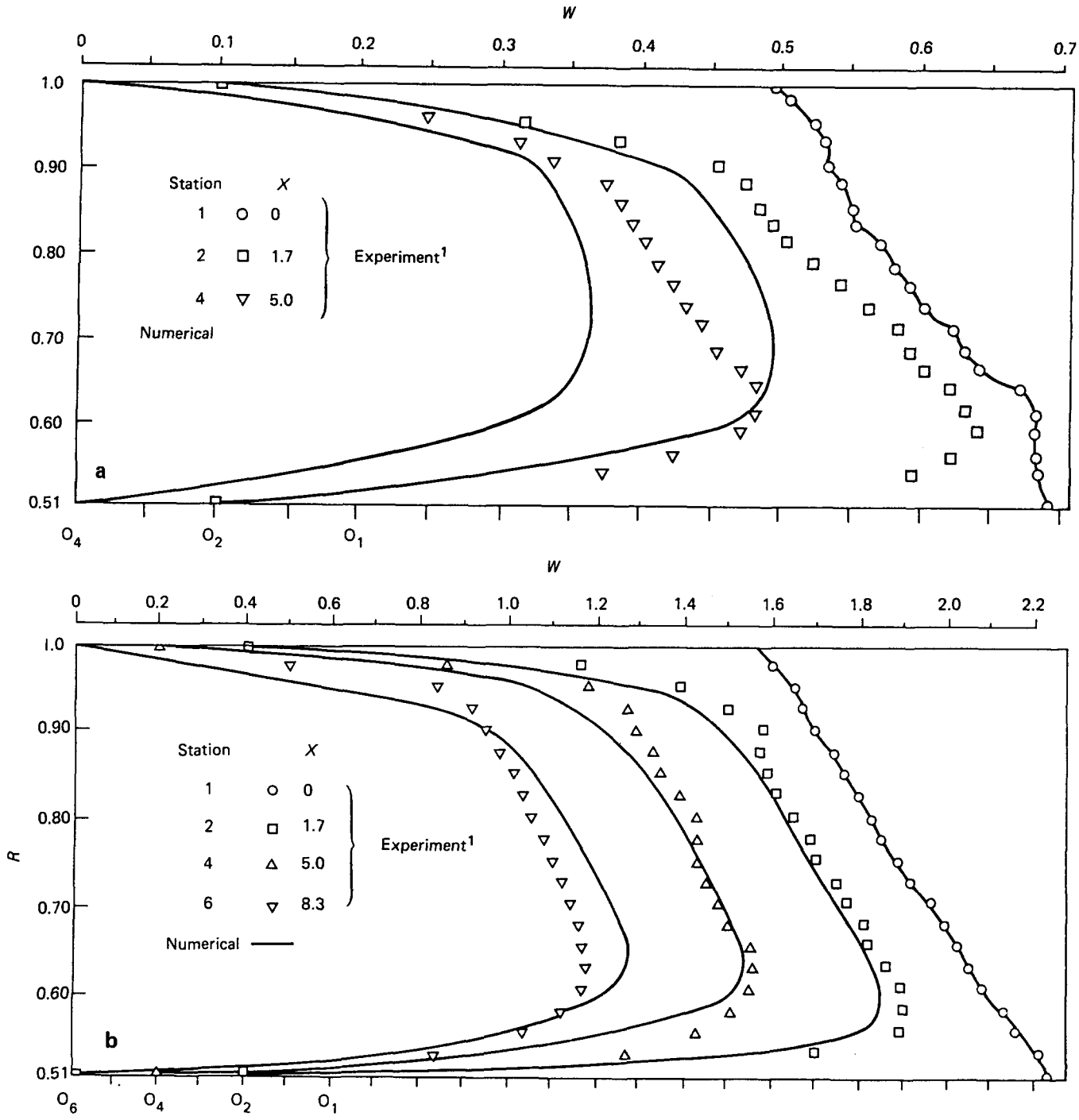

Fig 8 Tangential velocity profiles in annulus for $\alpha = 0.51$, Re $= 28\,700$ with swirl generator blade set at (a) 15°, (b) 45°. Numerical predictions assume constant effective viscosity

of axial velocity profiles was less satisfactory. To yield an improvement, the treatment of flow near the walls was carried out according to Eq (44). In the core region, where the flow is fully turbulent, a constant scalar turbulent viscosity was still used.

Figs 8(a) and 8(b) show the comparison between predictions and experiment for tangential velocity profiles with the swirl generator blades[1] set at 15° and 45° with $\alpha = 0.51$ and $Re = 28\,700$ in each case. Agreement is promising, especially for the higher swirl angle and over the first four stations, but discrepancies increase in magnitude further downstream.

The computed axial velocity variations across the annulus for several axial stations, corresponding to the conditions of Fig 8(a), are shown in Fig 9. Agreement with experiment is generally good near the outer wall, but significant departures can be seen as the inner wall is approached. Contrary to measurements, the theoretical profiles show a maximum velocity, for this constant viscosity analysis, slightly nearer the outer wall than the inner wall. Evidently, predictions of the U profiles could be improved. For the sake of comparison the fully developed laminar U profile for the swirl conditions described earlier is included in Fig 9. Time-mean velocity

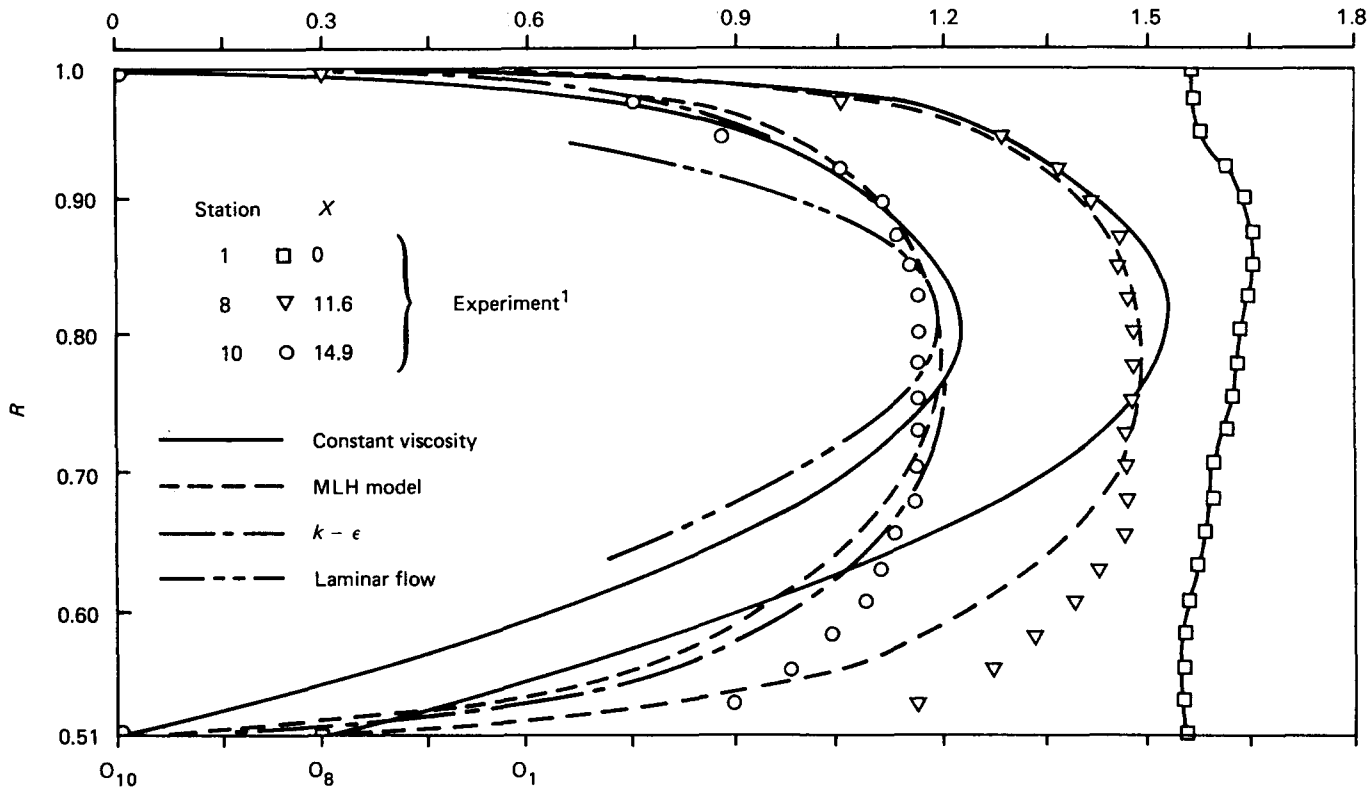

Fig 9 Axial velocity profiles for swirl generator blade set at 15° and Re = *28 700 using three different turbulence models. Fully developed laminar profile for conditions in Fig 6 shown for comparison*

measurements[1,9] have shown that axial velocity profiles are only slightly affected by swirl. Furthermore, it was concluded[9] that axial diffusivity is unaffected by swirl, which suggests that the equations that govern the axial velocity (vorticity and stream function equations) could be handled separately. In addition, non-isotropic turbulence could be introduced and, for the sake of simplicity, $\mu_{e,x}$ was calculated from Eq (12) in which the mixing length was defined as

$$l_x = C_x(r_o - r_i) \tag{55}$$

and the constant $C_x = 0.14$. However, for the swirl equation, the expression (54) was still used. An obvious improvement in the predictions can be seen as indicated by the MLH curves in Fig 9. The tangential velocity profiles remained unchanged with this analytical procedure.

The MLH model was also used to estimate the tangential eddy viscosity across the annulus using Eq (13). The choice of mixing length constants was derived from the optimization of experimental data. In the core region it was concluded that

$$l_\theta = 0.098(r_o - r_i) \tag{56}$$

for best results, but near the walls it was assumed that $l_x = l_\theta$ and the effective viscosity obtained from Eqs (51) and (12). Figs 10(a) and 10(b) show the tangential velocity profiles corresponding to this case for the experimental conditions of $\alpha = 0.51$, $Re = 28\,700$ and two swirl conditions at inlet.

Although agreement between theory and experimental data is not perfect, the degree of accuracy achieved could well match the requirements of many engineering applications.

The k–ε model was used to assess predictions for large inlet swirl velocities and, in particular, the swirl distribution generated by the swirl blades set at 45° and 15° for $Re = 28\,700$ and $\alpha = 0.51$. The previously discussed boundary conditions at inlet, on the walls and at outlet, were used for all the dependent variables with inlet data taken from experiments[1]. Fig 11 shows the comparison between experimental and numerically predicted tangential velocity profiles for the 45° case for values of X between 0 and 11.6, ie about 80% of the length of the test section from inlet. Although the predictions appear to be good, it is worth bearing in mind that to achieve this accuracy five coefficients are associated with this model. The time required to adjust these coefficients to produce satisfactory correlation can be excessive, which reduces somewhat the utility and attractiveness of such a procedure.

Predictions for the axial velocity profile using the k–ε model are shown in Fig 9. Clearly, agreement is good near the outer wall and in the core region but there is significant deviation near the inner wall. This disparity can be traced to the probability that the universal law of the wall, assumed to hold near both solid boundaries, is actually only valid near the outer wall, a conclusion also reached by Brighton and Jones[22] and Yamamoto and Millar[8].

Bearing in mind the complexity of the problem investigated in this paper perfect agreement between the results of numerical integration of the Navier–Stokes equations and experimental data, over a wide range of geometric and fluid property parameters, is unlikely to be achieved. However, to demonstrate further the capability of the foregoing methods of approach for turbulent swirl flows along axisymmetric annuli, two further examples are considered:

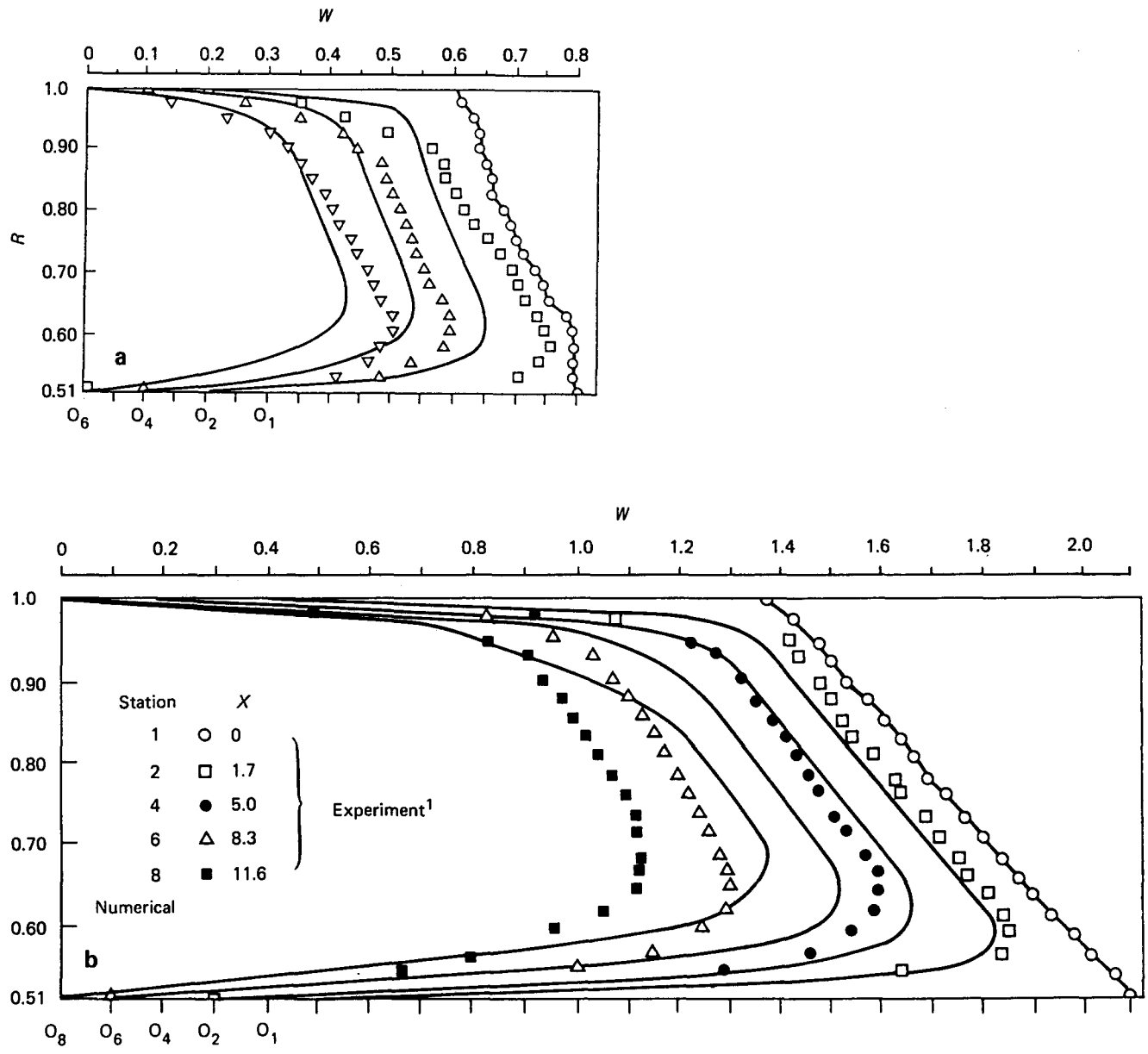

Fig 10 Tangential velocity profiles using a mixing length model for swirl generator blade angle set at (a) 15°, (b) 45°, and Re = *28 700*

(a) free vortex inlet swirl distribution given by $W = R^{-1}$ and $U = 1.0$;
(b) an experimental swirl distribution corresponding to a swirl blade angle of 15°.

Both the above flows were investigated for $Re =$ 28 700 and $\alpha = 0.51$, and the predicted results for the tangential velocity profiles are shown, respectively, in Figs 12 and 13. The calculations have been carried out to an equivalent station 21 corresponding to $X = 33.1$, ie more than twice the length of the test section over which measurements were made[1,2]. These and the previous figures demonstrate the success of the analytical techniques in predicting the principal characteristics of swirling flow along an axisymmetric annulus, namely:

(a) $\partial W/\partial R$ is large and positive near the inner wall;
(b) W then increases more slowly to a maximum;
(c) the maximum value of W migrates towards the outer wall with increasing distance downstream, and far downstream is located near mid-radius;
(d) $\partial W/\partial R$ is large and negative near the outer wall and is of smaller magnitude than the gradient near the inner wall in the early stages of flow development, but the behaviour reverses well downstream;
(e) in the core region $\partial W/\partial r$ is constant and negative, especially evident for modest inlet swirl where the condition exists well downstream before the W profile becomes a parabolic shape;
(f) other than in the immediate vicinity of inlet the U profile is little affected by swirl;
(g) radial velocities are always small for the inlet swirl distributions examined in this work.

It may also be noted, by comparing the data in Figs 6 and 12, that W decays far more rapidly in turbulent flow than in laminar flow. The preceding points (a) to (e) are clearly evident in Fig 6.

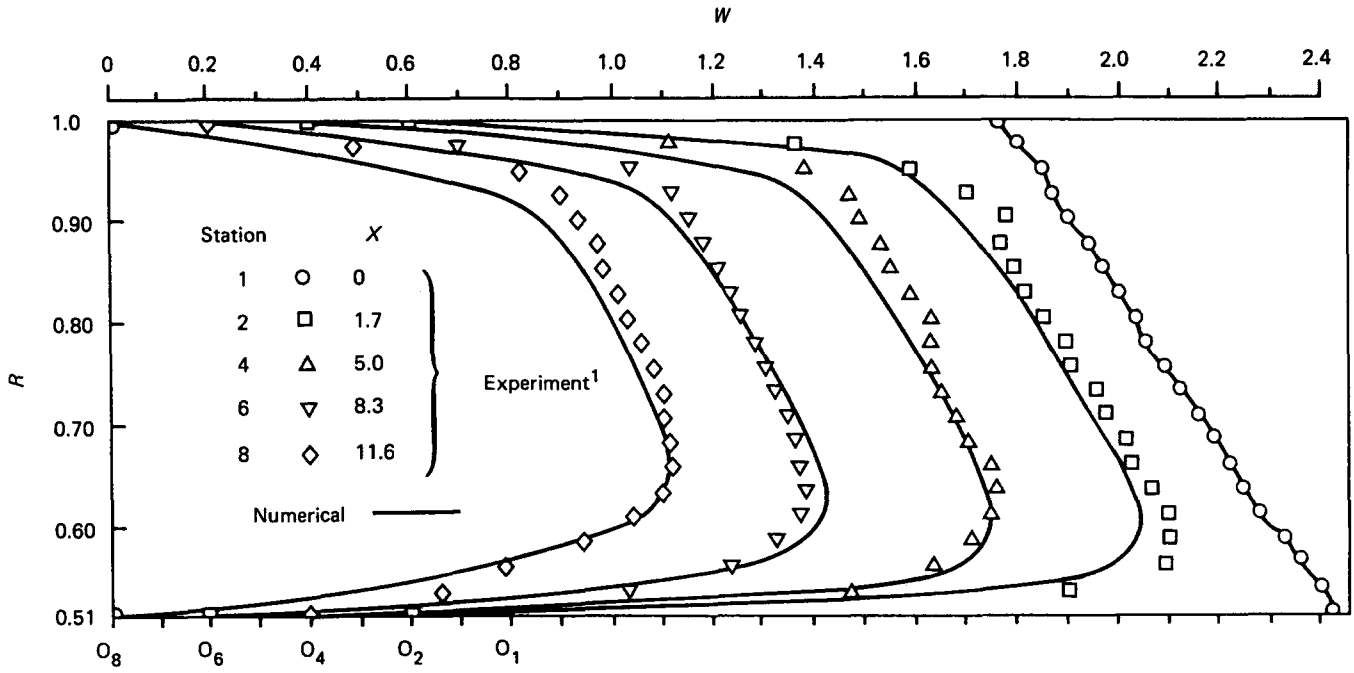

Fig 11 Tangential velocity profiles using a k–ε *model for swirl generator blade angle set at 45° and* Re = *28 700*

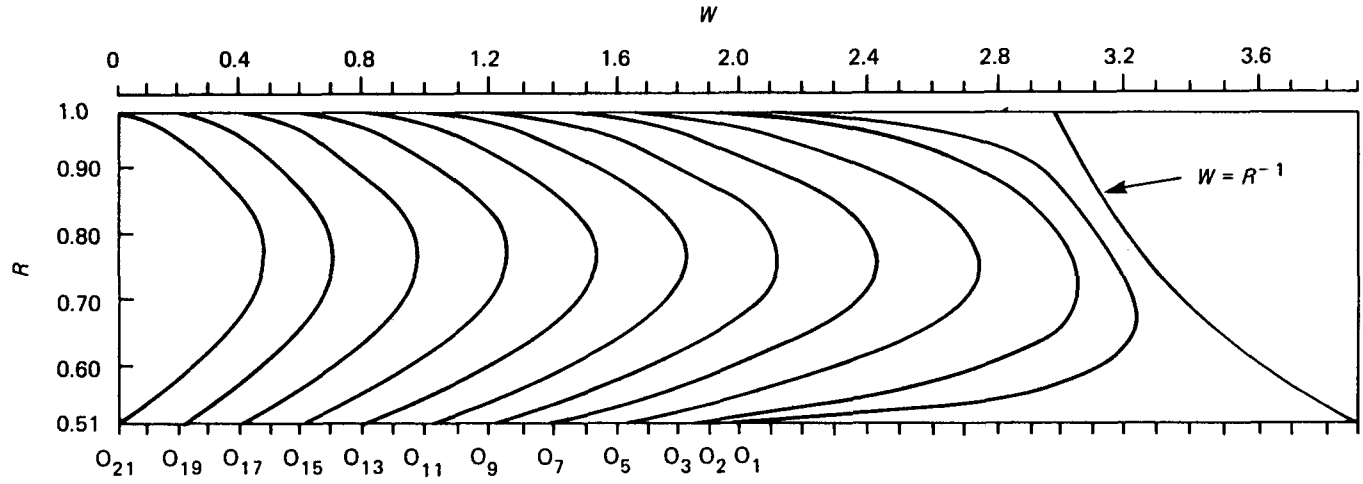

Fig 12 Predicted tangential velocity distributions along annulus for free vortex inlet swirl and Re = *28 700*

From these critical areas of agreement between theory and experiment it is considered that the present analytical approaches represent a generally valid means of predicting the behaviour of swirling turbulent flow that enters and subsequently decays along an axisymmetric annulus.

Conclusions

The principal conclusions that may be drawn from the foregoing analyses, in relation to previously reported experimental data, are as follows.

(a) Time-mean flow distributions can be predicted from finte difference solutions of equations that represent the minimum simplification of the steady-state Navier–Stokes equations describing turbulent swirling flow in an axisymmetric annulus.

(b) The accuracy of results depends critically on how well the boundary conditions used in the computations match the real conditions on the annulus walls.

(c) Numerical stability of such complex computations presents difficulties, including divergence, and these are exacerbated as interest moves from laminar to turbulent flow and from a pipe to an annulus. Under-relaxation techniques reduce the problem but as yet no general technique for choosing a relaxation factor is available.

(d) The convergence criterion should be chosen with care. Too small a value leads to more grid points and slower convergence, thus rapidly increasing computation time.

(e) For the Reynolds numbers considered, the precise boundary conditions far downstream have little effect on behaviour of the flow to at least $X = 15$, beyond which the flow becomes fully developed.

(f) A comparison with other work shows that, although more troublesome to analyse, the elliptic type of differential equations solved by finite difference

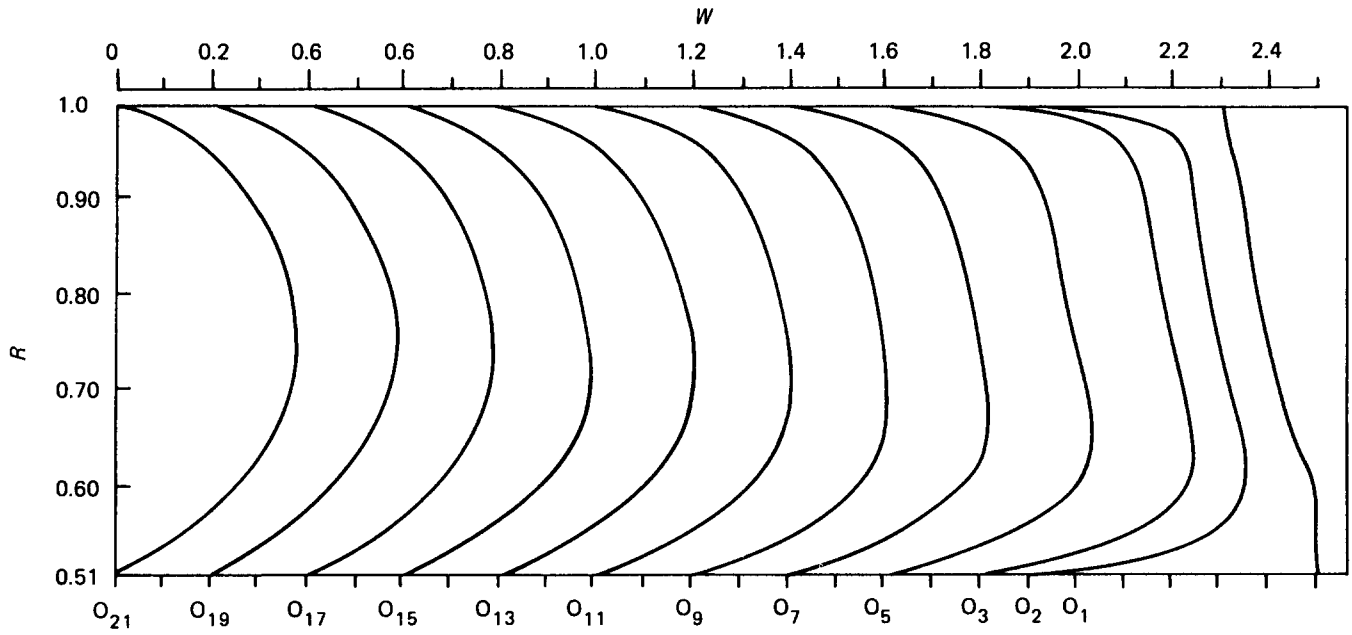

Fig 13 Predicted tangential velocity distributions along annulus for swirl generator blades set at 15° and Re = *28 700*

techniques, as herein, yield more accurate results than equations obtained in parabolic form.

(g) The isotropic turbulence (constant μ_e) assumption yields poor predictions; but, with careful treatment of wall conditions, reasonable predictions can be made with constant $\mu_{e,\theta}$ and mixing length estimations for $\mu_{e,x}$.

(h) The MLH models, with simple mixing length distributions, have been established from which time mean velocity profiles can be deduced that show reasonable agreement with experiments.

(i) The k–ε turbulence models can be made to fit experimental data well, but this requires continual input from such data. The appropriate coefficients need to be optimized for swirl flows as functions of inlet swirl profile, radius ratio, Reynolds number etc but this calls for further detailed study.

References

1. **Clayton B. R. and Morsi Y. S. M.** Determination of principal characteristics of turbulent swirling flow along annuli—Part 1: Measurement of time mean parameters. *Int. J. Heat and Fluid Flow, 1984*, **5**(*4*), *195–203*
2. **Clayton B. R. and Morsi Y. S. M.** Determination of principal characteristics of turbulent swirling flow along annuli—Part 2: Measurment of turbulence components. *Int. J. Heat and Fluid Flow, 1985*, **6**(*1*), *31–41*
3. **Sharma B. I., Launder B. E. and Scott C. J.** Computation of annular turbulent flow with rotating core tube. *J. Fluid Eng., Trans ASME, 1976*, **98**, *753–758*
4. **Morsi Y. S. M.** Analysis of turbulent swirling flows in axisymmetric annuli. *PhD Thesis, University of London, 1983*
5. **Scott C. J.** A series solution for decay of swirl in an annulus. *J. Appl. Mech., Trans ASME, 1972*, **39**(*94*), *289–290*
6. **Kreith F. and Sonju O. K.** The decay of turbulent swirling flow in a pipe. *J. Fluid Mech., 1965*, **22**, *257–271*
7. **Patankar S. V. and Spalding D. B.** *Heat and Mass Transfer in Boundary Layers, Intertext Books, London, 1970*
8. **Yamamoto A. and Millar D. A. J.** Calculation of laminar and turbulent swirling flows in cylindrical annuli. *ASME/AIChE Pub., Winter Annual Meeting, New York, 1979, 89–98*
9. **Scott C. J. and Rask D. R.** Turbulent viscosity for swirling flow in a stationary annulus. *J. Fluid Eng., Trans ASME, 1973*, **95**, *557–566*
10. **Gosman A. D., Pun W. M., Runchal A. K., Spalding D. B. and Wolfstein M. W.** *Heat and Mass Transfer in Recirculating Flows, Academic Press, London, 1969*
11. **Kubo I. and Gouldin F. C.** Numerical calculation of turbulent swirling flow. *J. Fluid Eng., Trans ASME, 1975*, **97**, *310–315*
12. **Crane C. M. and Burley D. M.** Numerical studies for viscous swirling flow through annular diffusers – Part 1: Method. *J. Eng. Math., 1974*, **8**, *181–192*
13. **Huang F. and Tsou F. K.** Friction and heat transfer in turbulent free swirling flow in pipes. *ASME/AIChE Pub., Natl. Heat Transfer Conf., Santiago, California, 1979*
14. **Rodi W.** Examples of turbulence models for incompressible flows. *AIAA J., 1982*, **20**, *872–879*
15. **Jones W. P. and Launder B. E.** The prediction of laminarisation with a two-equation model of turbulence. *Int. J. Heat Mass Transfer, 1972*, **15**, *301–315*
16. **Harlow F. W. and Nakayama P. I.** *Transport of Turbulence Energy Decay Rate, Los Alamos Sci. Lab., University of California Rep. LA-3854, 1968*
17. **Okhio C. B.** *Swirling Flow Through Conical Diffusers, PhD Thsis, University of London, 1982*
18. **Gosman A. D. and Pun W. M.** *Lecture notes for course entitled 'Calculation of Recirculating Flows', Dept. of Mech. Eng., Imperial College, London, Report HTS/74/2, 1974*
19. **Van Driest E. R.** On turbulent flow near a wall. *J. Aeronaut. Sci., 1957*, **23**, *1007*
20. **Goldstein S.** *Modern Developments in Fluid Dynamics, Clarendon Press, Oxford, 1938*
21. **Schlichting H.** *Boundary Layer Theory, McGraw-Hill, New York, 1979*
22. **Brighton J. A. and Jones J. B.** Fully-developed turbulent flow in annuli. *J. Basic Eng., Trans ASME, 1964*, **86**, *835–844*
23. **Hanjalic K. and Launder B. E.** A Reynolds stress model of turbulence and its application to thin shear flows. *J. Fluid Mech., 1972*, **52**, *609–638*